Journal of Materials Processing Technology 210 (2010) 204–211

Contents lists available at ScienceDirect

Journal of Materials Processing Technology

journal homepage: www.elsevier.com/locate/jmatprotec

Sensitivity of material properties on distortion and residual stresses during metal quenching processes

Ashok Kumar Nallathambi[a,*], Yalcin Kaymak[b], Eckehard Specht[a], Albrecht Bertram[a]

[a] Otto von Guericke University Magdeburg, 39106 Magdeburg, Germany
[b] VDEh-Betriebsforschungsinstitut GmbH, D-40237 Düsseldorf, Germany

ARTICLE INFO

Article history:
Received 13 March 2009
Received in revised form 1 July 2009
Accepted 3 September 2009

Keywords:
Quenching
Distortion
Residual stress
Sensitivity
FEM
Plasticity
Phase transformation

ABSTRACT

This research work investigates the influence of thermal, metallurgical and mechanical properties on the final distortion and residual stresses during metal quenching processes. The Finite Element Method (FEM) is employed to solve the coupled partial differential equations. The coupling effects such as phase transformation enthalpy, transformation-induced plasticity and dissipation are considered. The curvature and the volume averaged effective stresses are treated as a measure of distortion and residual stresses, respectively. Sensitivity analyses for the material parameters on the distortion and residual stresses are carried out. An L120 × 12 profile made of 100Cr6 steel is considered for the analyses. The sensitivity of the density, specific heat capacity, thermal conductivity, transformation start and end times, martensitic transformation coefficient, martensite start temperature, bulk modulus, shear modulus, yield strength and hardening modulus are of main concern in this work. It is found that reduced metallurgical properties, yield stress, and bulk modulus simultaneously lower the distortion and residual stresses for an equal cooling.

© 2009 Elsevier B.V. All rights reserved.

1. Introduction

Quenching is an important heat treatment process in many industrial fields for obtaining the desired metallurgical and mechanical properties. However, modeling of quenching processes is quite complicated and cumbersome due to the couplings of thermal, metallurgical, and mechanical fields as shown in Fig. 1. The temperature field controls the phase transitions and thermal strains while the transformation latent heat and dissipation produces additional heat that alters the temperature field. Furthermore, the phase transformations control the displacement field by transformation-induced plastic strains and dilatation upon density variation. Apart from the quenchant and Heat Transfer Coefficient (HTC) profile (Totten et al., 1993), the complete quenching process depends on the thermal, metallurgical, and mechanical material properties. This research work studies the influence of the material properties on the distortion and residual stresses produced during the quenching process.

Sjostrom (1984) reported that the transformation kinetics has little influence on the state of stress. Todinov (1999) studied the influences of the martensitic start temperature and the martensitic transformation temperature interval on residual stresses. Batista and Kosel (2000) conducted the sensitivity analysis for predicting the errors in the residual stresses from the estimated errors in the material data during the heat treatment of steel. Ferguson et al. (2001) showed that identical phase distributions can produce very different residual stress patterns based on timing of the phase changes and also relative location within a given steel part. Song et al. (2003) introduced a sensitivity coefficient based sensitivity analysis of the thermomechanical response of welded joints. In Song et al. (2003), the first- and second-order sensitivity coefficients of the thermal and mechanical response quantities are evaluated using a direct differentiation approach. Chuzhoy et al. (2003) performed the sensitivity studies to identify the influence of quench characterization on simulation results. Friesenbichler et al. (2006) pointed out the sensitivity of material data on phase transformation and residual stresses during hardening. Recently, Mirzaee-Sisan et al. (2007), Barka et al. (2007), Li et al. (2007), and Freborg et al. (2007) attempted the sensitivity studies for fitting the experimental results. This work introduces a simple sensitivity analysis which reveals the impact of important material properties on the distortion and residual stresses.

Our previous works (Pietzsch et al., 2005, 2007; Brzoza et al., 2006; Kaymak and Specht, 2007; Kaymak, 2007; Nallathambi et al., 2008, 2009) are focused to the optimum cooling strategies through a modified HTC profile which reduces the distortion and

* Corresponding author at: Institute of Fluid Dynamics and Thermodynamics (ISUT), Otto von Guericke University Magdeburg, Universitätsplatz 2, G10-132, 39106 Magdeburg, Germany. Tel.: +49 391 67 12737.
E-mail address: ashok.nallathambi@st.ovgu.de (A.K. Nallathambi).

0924-0136/$ – see front matter © 2009 Elsevier B.V. All rights reserved.
doi:10.1016/j.jmatprotec.2009.09.001

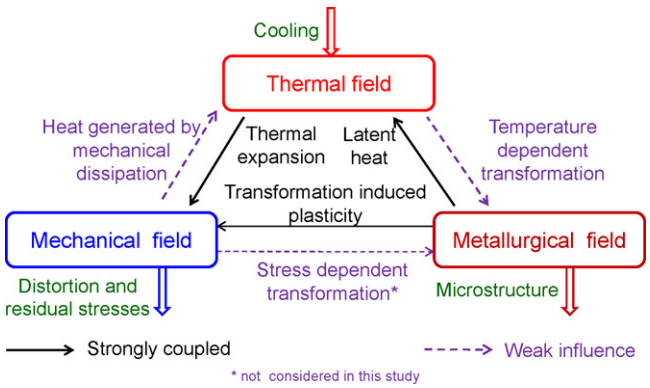

Fig. 1. Schematic representation of various couplings between physical fields.

residual stresses simultaneously. Apart from the external parameters which control the quenching process, the internal parameters which significantly dominate in the quenching process are the material properties. The sensitivity analysis is useful for the understanding of the influence of different material properties which control the quenching processes. It is also possible to modify the material properties upto a certain extent through proper alloying. Therefore, an attempt is made to identify the key material properties which simultaneously reduces the distortion and residual stresses. The mathematical aspects of various physical fields are discussed in Section 2. The finite element discretization of governing equations of various fields are discussed in Section 3. In Section 4, the results of sensitivity analysis is presented by a numerical example.

2. Mathematical formulation

During the quenching process, the temperature, microstructure, and stresses at every material point change with respect to time. The *metal quenching* problem consists of finding the absolute temperature field θ, phase fractions f_j and displacement $\vec{u}$ at every material point ($\vec{X}$) such that (Kaymak, 2007)

$$-\nabla\cdot\vec{q}+\chi\sigma_y\dot{\epsilon}^p+\sum_{j=1}^{n_p}L_j\dot{f}_j=\rho c_p\dot{\theta} \tag{1}$$

$$\nabla\cdot\mathbf{T}+\vec{b}=\vec{0} \tag{2}$$

are fullfilled. The phase transformations are

$$\dot{f}_P=\frac{1}{t_e(\theta)-t_s(\theta)}\qquad \text{if Schiel' s sum} \geq 1 \tag{3}$$

$$f_M=f_A\{1-\exp[k_M(\theta-M_s)]\}\quad \text{if}\quad \theta<M_s \tag{4}$$

subject to the essential boundary conditions (BC)

$$\theta=\theta_s\quad \text{in}\quad \Gamma_\theta \tag{5}$$

$$\vec{u}=\vec{u}_s\quad \text{in}\quad \Gamma_u \tag{6}$$

and the natural BC

$$\vec{q}\cdot\vec{n}=q_s\quad \text{in}\quad \Gamma_q \tag{7}$$

$$\mathbf{T}\cdot\vec{n}=\vec{t}\quad \text{in}\quad \Gamma_t \tag{8}$$

and the initial conditions

$$\begin{aligned}\theta(\vec{X},t)|_{t=0}&=\theta_0(\vec{X})\\ \mathbf{T}(\vec{X},t)|_{t=0}&=\mathbf{0}\end{aligned} \tag{9}$$

Eqs. (1) and (2) represent the energy balance and conservation of linear momentum, respectively. The superimposed dot denotes time derivative, and ∇ is the gradient operator with respect to Cartesian reference system. In Eq. (1), ρ is the density, c_p is the specific heat capacity, $\vec{q}$ is the heat flux vector, χ is the fraction of mechanical energy converted into thermal energy (Argyris and Doltsinis, 1981), σ_y is the yield strength, $\dot{\epsilon}^p$ is the rate of effective plastic strain, L_j is the latent heat of the individual phase transformation, $\dot{f}_j$ is the phase transition rate and n_p is the number of product phases. In Eq. (2), $\mathbf{T}$ is the stress tensor and $\vec{b}$ is the body force vector.

In this work, the following three phases are assumed: austenite (A), pearlite (P), and martensite (M). During the time-dependent diffusive transformation, the austenite transforms into pearlite and is modeled by a linear iso-kinetic law (Kaymak, 2007) with the help of an isothermal transformation diagram (Johnson and Mehl, 1939; Avrami, 1939) which is obtained from the TTT diagram (for more details we refer to Kang and Im, 2007) along with Schiel's additivity rule (Scheil, 1935) as given in Eq. (3). In Eq. (3), t_s and t_e are the transformation start and end times, respectively. During the displacive transformation, the austenite gets transformed into martenstie and modeled using the KM law (Koistinen and Marburger, 1959) as given in Eq. (4). In Eq. (4), M_s is the martensite start temperature and k_M (≈ 0.011 for steel) is the stress dependent transformation constant.

The boundary conditions form a restriction: $\Gamma=\Gamma_\theta\cup\Gamma_q=\Gamma_u\cup\Gamma_t$. In the essential BC Eqs. (5) and (6), θ_s is the prescribed surface temperature, and $\vec{u}_s$ is the prescribed displacement vector. Similarly, in the natural BC Eqs. (7) and (8), q_s is the normal heat flux due to convection–radiation phenomenon and $\vec{t}$ is the prescribed traction vector with unit outward normal $\vec{n}$. From the Fourier's law of heat conduction, the heat flux can be related as

$$\vec{q}=-k(\theta,f_j)\nabla\theta \tag{10}$$

where k is the temperature and phase fraction-dependent thermal conductivity. On the heat flux boundary Γ_q, q_s is the normal heat flux due to convection-radiation phenomenon and can be stated according to Newton's law of convection as

$$q_s=\alpha(\theta)(\theta-\theta_\infty) \tag{11}$$

where α is the HTC and θ_∞ is the ambient temperature. The initial high temperature $\theta_0(\vec{X})$ and zero initial stress tensor $\mathbf{0}$ are treated as initial conditions in Eq. (9).

Using a small deformation theory, the total strain $\mathbf{E}$ can be additively decomposed into four components as (Pietzsch et al., 2007)

$$\mathbf{E}=\frac{1}{2}[\nabla\vec{u}+(\nabla\vec{u})^T]=\mathbf{E}^e+\mathbf{E}^p+\mathbf{E}^{\text{tp}}+\mathbf{E}^{\text{trip}} \tag{12}$$

where $\mathbf{E}^e$ is the elastic strain tensor, $\mathbf{E}^p$ is the plastic part of strain tensor, $\mathbf{E}^{\text{trip}}$ is the transformation-induced plastic (TRIP) strain tensor and $\mathbf{E}^{\text{tp}}$ is the volumetric strain tensor due to temperature and phase changes. Instead of using the coefficient of thermal expansion (Smoljan, 2002; Andrade-Campos et al., 2007), $\mathbf{E}^{\text{tp}}$ is expressed in terms of reference density ρ_R and current density $\rho(\theta,f_j)$ of the mixture

$$\mathbf{E}^{\text{tp}}=\left(\sqrt[3]{\frac{\rho_R}{\rho(\theta,f_j)}}-1\right)\mathbf{I} \tag{13}$$

The TRIP strain rate can be calculated from the macroscopic material behavior based on the micro-mechanical approach and is given

as in Kaymak (2007)

$$\dot{\mathbf{E}}^{\text{trip}} = -\frac{3}{2}\mathbf{T}'\sum_{j=1}^{n_p}\{\Lambda_j \text{SF}(f_j)\dot{f}_j\} \tag{14}$$

where SF is the Saturation Function (Leblond, 1989) (the natural logarithmic function is used in this work), and Λ_j is the Greenwood–Johnson (GJ) coefficient (Greenwood and Johnson, 1965) which must be determined experimentally. The GJ coefficient expresses the compensation of the volume mismatch which produces a plastification in a phase transformation micro-region.

When the equivalent stress exceeds the yield stress, plastic strain occurs. Using a classical rate-independent (Chen, 1994), isotropic, thermo-plastic material model with temperature and phase fraction-dependent constitutive law, the plastic strain can be estimated systematically employing the yield criterion, the loading criterion, the flow rule, the hardening rule and consistency condition. The constitutive law of the isotropic material can be written as in Simo and Hughes (1997)

$$\mathbf{T} = \mathbb{C}^e : \mathbf{E}^e = \kappa\,\text{tr}(\mathbf{E} - \mathbf{E}^{\text{tp}})\mathbf{I} + 2\mu(\mathbf{E}' - \mathbf{E}^{\text{trip}} - \mathbf{E}^p) \tag{15}$$

where $\mathbb{C}^e$ is the fourth-order elasticity tensor (Bertram et al., 2007), κ is the bulk modulus and μ is the shear modulus, altogether functions of temperature and phase fractions. The isotropic hardening rule can be stated as

$$\sigma_y(\epsilon^p, \theta, f_j) = \sigma_{yo}(\theta, f_j) + H(\theta, f_j)\epsilon^p \tag{16}$$

where σ_{yo} is the initial yield stress, ϵ^p is the effective plastic strain, and H is the hardening modulus.

3. Solution methodology

The FEM is implemented for the solution of the thermal and mechanical equilibrium equations. Non-linear coupled simultaneous equations obtained through FEM are solved using isothermal staggered algorithm (Armero and Simo, 1992). Thermal, metallurgical and mechanical fields are solved sequentially in every time step in the following way:

1. The thermal field is solved at a fixed configuration and phase fractions.
2. The metallurgical field is solved at a fixed configuration and constant temperature.
3. The mechanical field is solved at a constant temperature and phase fractions.

In each time step, first the transient temperature field is solved iteratively, then the phase transitions are computed, and finally the displacement field is computed iteratively using full Newton–Raphson method. The discrete form of all coupled equations are derived and discussed in detail in the following subsections.

3.1. Thermal field formulation

For an arbitrarily chosen temperature distribution $\tilde{\theta}$, the thermal equilibrium condition in Eq. (1) has to satisfy the following integral based on virtual temperature principle as

$$\int_\Omega \left[\nabla\cdot(k\nabla\theta) + \chi\sigma_y\dot{\epsilon}^p + \sum_{j=1}^{n_p} L_j\dot{f}_j - \rho c_p\dot{\theta}\right]\tilde{\theta}\,\mathrm{d}\Omega = 0 \tag{17}$$

Applying the Gauss divergence theorem on natural thermal boundary condition Eq. (7) and substituting Eq. (11) in Eq. (17) and it becomes

$$\int_\Omega [\nabla\tilde{\theta}\cdot(k\nabla\theta)]\,\mathrm{d}\Omega + \int_\Omega [\tilde{\theta}\rho c_p\dot{\theta}]\,\mathrm{d}\Omega + \int_{\Gamma_q}[\tilde{\theta}h\theta]\,\mathrm{d}\Gamma_q$$
$$= \int_\Omega \left[\tilde{\theta}\left(\chi\sigma_y\dot{\epsilon}^p + \sum_{j=1}^{n_p} L_j\dot{f}_j\right)\right]\mathrm{d}\Omega + \int_{\Gamma_q}[\tilde{\theta}h\theta_\infty]\,\mathrm{d}\Gamma_q \tag{18}$$

Using standard isoparametric element interpolation technique, element temperature θ_e and its spatial gradients are given as

$$\begin{aligned}\theta_e &= \mathbf{N}^T\boldsymbol{\Theta}_e\\ \nabla\theta_e &= \nabla\mathbf{N}^T\boldsymbol{\Theta}_e = \mathbf{H}\boldsymbol{\Theta}_e\end{aligned} \tag{19}$$

where $\mathbf{N}$ is the element shape function, $\boldsymbol{\Theta}_e = \{\theta_1, \theta_2, \ldots, \theta_\beta\}^T$ is the element nodal temperature vector, β is the number of nodes per element in the thermal problem, and $\mathbf{H}$ is the element temperature-gradient interpolation operator. Substituting Eq. (19) in Eq. (18), $\tilde{\boldsymbol{\Theta}}_e$ can be eliminated from both sides. Using the implicit Euler backward time difference scheme, the nodal temperature vector and its time derivatives for the current iteration $(i+1)$ and current time step $(t+\Delta t)$ are given as

$$\begin{aligned}\boldsymbol{\Theta}_{i+1}^{t+\Delta t} &= \boldsymbol{\Theta}_i^{t+\Delta t} + \Delta\boldsymbol{\Theta}\\ \dot{\boldsymbol{\Theta}}_{i+1}^{t+\Delta t} &= \frac{\boldsymbol{\Theta}_i^{t+\Delta t} + \Delta\boldsymbol{\Theta} - \boldsymbol{\Theta}^t}{\Delta t}\end{aligned} \tag{20}$$

Utilizing Eq. (20) in the previous equation, the final matrix form of thermal equilibrium is given as

$$\left\{\mathbf{K}^{\theta}{}_i^{t+\Delta t} + \frac{1}{\Delta t}\mathbf{C}^{\theta}{}_i^{t+\Delta t}\right\}(\Delta\boldsymbol{\Theta}) = \mathbf{F}^{\theta\,t+\Delta t} - \mathbf{R}^{\theta}{}_i^{t+\Delta t} \tag{21}$$

where $\mathbf{K}^\theta$ is the global conductance matrix, $\mathbf{C}^\theta$ is the global capacitance matrix, $\mathbf{F}^\theta$ is the global thermal force vector, and $\mathbf{R}^\theta$ is the global residual thermal force vector. The elemental form of these matrices and vectors are given as in Bathe (1996)

$$\begin{aligned}\mathbf{K}_{ei}^{\theta\,t+\Delta t} &= \int_\Omega [\mathbf{H}^T k_i^{t+\Delta t}\mathbf{H}]\,\mathrm{d}\Omega + \int_{\Gamma_q}[\mathbf{N}^S h_i^{t+\Delta t}(\mathbf{N}^S)^T]\,\mathrm{d}\Gamma_q\\ \mathbf{C}_{ei}^{\theta\,t+\Delta t} &= \int_\Omega [\mathbf{N}\rho_i^{t+\Delta t}c_{p_i}{}^{t+\Delta t}\mathbf{N}^T]\,\mathrm{d}\Omega\\ \mathbf{F}_i^{\theta\,t+\Delta t} &= \int_\Omega \left[\mathbf{N}\left(\chi\sigma_y\dot{\epsilon}^p + \sum_{j=1}^{n_p} L_j\dot{f}_j\right)_i^{t+\Delta t}\right]\mathrm{d}\Omega + \int_{\Gamma_q}[\mathbf{N}h_i^{t+\Delta t}\theta_\infty]\,\mathrm{d}\Gamma_q\\ \mathbf{R}_{ei}^{\theta\,t+\Delta t} &= \left\{\int_\Omega [\mathbf{H}^T k_i^{t+\Delta t}\mathbf{H}]\,\mathrm{d}\Omega\right\}\boldsymbol{\Theta}_{ei}{}^{t+\Delta t} + \mathbf{C}_{ei}^{\theta\,t+\Delta t}\left(\frac{\boldsymbol{\Theta}_{ei}{}^{t+\Delta t} - \boldsymbol{\Theta}_e{}^t}{\Delta t}\right)\end{aligned} \tag{22}$$

3.2. Phase field formulation

At the end of thermal field computation, the current temperature $\theta^{t+\Delta t}$ and current temperature increment $\Delta\theta = \theta^{t+\Delta t} - \theta^t$ are known at every integration point of the elements. The displacive and diffusive phase transitions are computed using these temperature details.

3.2.1. Diffusive phase transitions

In this work, pearlite is considered as the only product of diffusive transformation which is a reasonable simplification. Scheil's sum increment ΔS at the current time step can be computed using the IT diagram informations and given as in Kaymak (2007)

$$\Delta S = \frac{\Delta t}{t_s{}^{t+0.5\Delta t}} \tag{23}$$

The current Scheil's sum can be updated to $S^{t+\Delta t} = S^t + \Delta S$. The general phase fraction evolved during the current time step can be given as

$$\Delta f = \frac{\zeta \Delta t}{{t_e}^{t+0.5\Delta t} - {t_s}^{t+0.5\Delta t}} \tag{24}$$

The following three possibilities arise in this calculation:

- If $S^{t+\Delta t} < 1$, then $\Delta f = 0$.
- If $S^t < 1$ and $S^{t+\Delta t} > 1$, the incubation time is reached during the current time step, and only a fraction ζ of Δt contributes to phase transition and $\zeta \approx \frac{S^{t+\Delta t}-1}{\Delta S}$.
- If $S^{t+\Delta t} > 1$ and also $S^t > 1$, the phase transition already started and $\zeta = 1$, since the full time step contributes to phase transition.

3.2.2. Displacive phase transitions

The stress dependency of the martensitic transformation coefficient k_M in Eq. (4) can be included in the model by introducing additional stress coefficients given as

$$f_M^{t+\Delta t} = f_A^{t+\Delta t}\{1 - \exp[k_M(\theta^{t+\Delta t} - M_s) - a_{\sigma m}{\sigma_m}^t - a_{\sigma e}{\sigma_{eff}}^t]\} \tag{25}$$

where $a_{\sigma m}$ and $a_{\sigma e}$ are material parameters for the martensitic transformation which demand experimental evaluation, σ_m and σ_{eff} are the mean and effective stresses at previous time step. For the sake of simplicity, $a_{\sigma m}$ and $a_{\sigma e}$ can be assumed as zero.

3.3. Displacement field formulation

Following the same arguments used in the thermal field, for an arbitrary displacement field $\tilde{u}$, the mechanical equilibrium condition Eq. (2) has to satisfy the following integral equation

$$\int_\Omega [\nabla \cdot \mathbf{T} + \vec{b}] \cdot \vec{\tilde{u}}\, \mathrm{d}\Omega = 0 \tag{26}$$

Using Gauss divergence theorem, the natural mechanical boundary condition Eq. (8) can be substituted in Eq. (26), and results in

$$\int_\Omega [\mathbf{T}{:}\tilde{\mathbf{E}}]\, \mathrm{d}\Omega = \int_{\Gamma_t} [\vec{t} \cdot \vec{\tilde{u}}]\, \mathrm{d}\Gamma_t + \int_\Omega [\vec{b} \cdot \vec{\tilde{u}}]\, \mathrm{d}\Omega \tag{27}$$

The x, y and z components of the element nodal displacements are given as

$$u_e = \mathbf{N}^T\mathbf{U}_e, \quad v_e = \mathbf{N}^T\mathbf{V}_e, \quad w_e = \mathbf{N}^T\mathbf{W}_e \tag{28}$$

where $\mathbf{N}$ is the element shape function. The element strains are

$$\mathbf{E}_e = \mathbf{B}\hat{\mathbf{U}}_e \tag{29}$$

where $\mathbf{B}$ is the strain–displacement matrix which is unique for the particular structural problem which will be discussed in Section 3.4. If ω is the number of nodes per element in the mechanical problem, the total elemental displacement degree of freedom vector ($\hat{\mathbf{U}}_e$) is expressed by

$$\hat{\mathbf{U}}_e = \{\, U_{e1} \quad V_{e1} \quad W_{e1} \quad \ldots \quad U_{e\omega} \quad V_{e\omega} \quad W_{e\omega}\,\}^T \tag{30}$$

where $\mathbf{U}_e$, $\mathbf{V}_e$ and $\mathbf{W}_e$ are the individual x, y and z directional displacement vectors. Substituting Eqs. (28) and (29) into Eq. (27), $\tilde{\hat{\mathbf{U}}}_e$ can be eliminated from both sides. The following incremental relations for every time step with current iteration $(i+1)$ are used:

$$\begin{aligned}
\Delta\mathbf{E}_e &= \mathbf{B}^T\Delta\hat{\mathbf{U}}_e \\
\Delta\mathbf{T}_e &= \mathbf{C}^{\mathrm{ep}\,t+\Delta t}_{i+1}\Delta\mathbf{E}_e \\
\hat{\mathbf{U}}_{e_{i+1}}^{t+\Delta t} &= \hat{\mathbf{U}}_{e_i}^{t+\Delta t} + \Delta\hat{\mathbf{U}}_e \\
\Delta\mathbf{T}_{e_{i+1}}^{t+\Delta t} &= \Delta\mathbf{T}_{e_i}^{t+\Delta t} + \mathbf{C}^{\mathrm{ep}\,t+\Delta t}_i\Delta\mathbf{E}_e
\end{aligned} \tag{31}$$

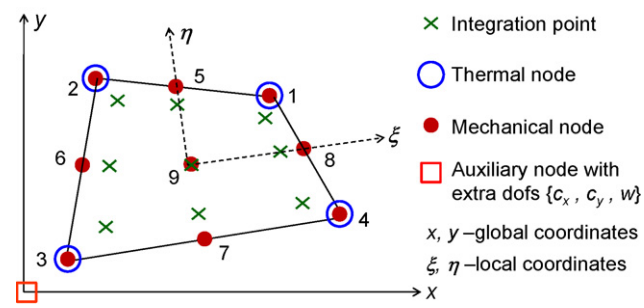

Fig. 2. Layout of a typical element.

where $\mathbf{C}^{\mathrm{ep}}$ is the elemental tangent elasto-plastic matrix (Simo and Hughes, 1997). At the beginning of the current time step

$$\begin{aligned}
{\mathbf{E}_e}_1^{t+\Delta t} &= {\mathbf{E}_e}^t + \Delta{\mathbf{E}_e}^{\mathrm{tp}} + \Delta{\mathbf{E}_e}^{\mathrm{trip}} \\
{\mathbf{T}_{e_1}}^{t+\Delta t} &= {\mathbf{T}_e}^t
\end{aligned} \tag{32}$$

the final global form of mechanical equilibrium equation becomes

$$\mathbf{K}^{u\,t+\Delta t}_i\Delta\hat{\mathbf{U}} = \mathbf{F}^{u\,t+\Delta t} - \mathbf{R}^{u\,t+\Delta t}_i \tag{33}$$

where $\mathbf{K}^u$ is the global stiffness matrix, $\mathbf{F}^u$ is the global equivalent nodal load vector and $\mathbf{R}^u$ is the internal reaction vector taken from the previous iteration. Elemental form of matrices and vectors are given as in Bathe (1996)

$$\begin{aligned}
\mathbf{K}_{e\,i}^{u\,t+\Delta t} &= \int_\Omega [\mathbf{B}^T\mathbf{C}^{\mathrm{ep}\,t+\Delta t}_i\mathbf{B}]\, \mathrm{d}\Omega \\
\mathbf{F}_e^{u\,t+\Delta t} &= \int_{\Gamma_f} [(\mathbf{N}^S)^T\mathbf{t}_e^{\,t+\Delta t}]\, \mathrm{d}\Gamma_f + \int_\Omega [\mathbf{N}^T\mathbf{b}_e^{\,t+\Delta t}]\, \mathrm{d}\Omega \\
\mathbf{R}_{e\,i}^{u\,t+\Delta t} &= \int_\Omega [\mathbf{B}^T\mathbf{T}_{e_i}^{t+\Delta t}]\, \mathrm{d}\Omega
\end{aligned} \tag{34}$$

where $\mathbf{t}_e$ is the boundary element traction vector, and $\mathbf{b}_e$ is the element body force vector.

3.4. Structural application

Thermal, metallurgical and mechanical field computations which are discussed in Section 3.1–3.3 are similar for any kind of a three dimensional metal quenching process except the calculation of strain–displacement matrix $\mathbf{B}$. The evaluation of $\mathbf{B}$ for a particular structure considered are discussed in this section.

The total strain is the derivative of the displacement field. Therefore, a linear total strain field is obtained for the 9-noded element. In order to have a linear stress field, the thermal strains must also be linear. Since the thermal strains are linear functions of temperature, the thermal field must also be linear. Such a linear thermal field can be provided by 4-noded elements. The typical element layout is indicated in Fig. 2.

Using an isoparametric element formulation, the global co-ordinates and displacements are given in terms of local co-ordinates (ξ, η) by

$$\left.\begin{aligned} x(\xi,\eta) &= \mathbf{N}^T\mathbf{X} \\ y(\xi,\eta) &= \mathbf{N}^T\mathbf{Y} \end{aligned}\right\} \quad \text{and} \quad \left.\begin{aligned} u(\xi,\eta) &= \mathbf{N}^T\mathbf{U}_e \\ v(\xi,\eta) &= \mathbf{N}^T\mathbf{V}_e \end{aligned}\right\}, \tag{35}$$

The derivatives of shape functions with respect to the global x and y co-ordinates are represented by the operator $\mathbf{H}$ of size 2×9 as

$$\mathbf{H} = \left\{\begin{matrix} \dfrac{\partial}{\partial x} \\ \dfrac{\partial}{\partial y} \end{matrix}\right\}\mathbf{N}^T = \mathbf{J}^{-T}\left\{\begin{matrix} \dfrac{\partial}{\partial \xi} \\ \dfrac{\partial}{\partial \eta} \end{matrix}\right\}\mathbf{N}^T. \tag{36}$$

The strain–displacement operator **B** (subscript '*e*' is suppressed) for the *plane stress problems* is the simplest one and it is refereed in this text as standard strain–displacement operator with size 3 × 18,

$$\mathbf{B} = \mathbf{B}_{\text{std}} = \left[\begin{array}{cc|c|cc} H_{x1} & 0 & \cdots & H_{x\omega} & 0 \\ 0 & H_{y1} & \cdots & 0 & H_{y\omega} \\ H_{y1} & H_{x1} & \cdots & H_{y\omega} & H_{x\omega} \end{array}\right] \tag{37}$$

where H_x and H_y are the elements of the first and second rows of derivative operator **H**.

In this work, a new *beam cross-sectional element* is introduced to analyze the long profiles which has one extra global node with 3 degrees of freedom as shown in Fig. 2. The strain–displacement matrix for the beam (Kaymak, 2007) case has the size 4 × 21. There is one additional row and three additional columns. The introduced addition is names as $\mathbf{B}_{\text{beam}}$ and

$$\mathbf{B} = \begin{bmatrix} \mathbf{B}_{\text{std}} & \mathbf{0} \\ \mathbf{0} & \mathbf{B}_{\text{beam}} \end{bmatrix}, \quad \text{where} \quad \mathbf{B}_{\text{beam}} = \frac{1}{\ell}[\,1 \quad y \quad -x\,] \tag{38}$$

The additional operator $\mathbf{B}_{\text{beam}}$ is only for computing the strain in the axial direction, which is just related to axial elongation w and bending curvatures c_x and c_y, and ℓ is considered as unity. c_x and c_y are the curvatures of the long profile about the x- and y-axis, respectively. In this way, one can avoid the cumbersome 3D analysis. For the non-uniform cross-sections, the y-axis is assigned in the symmetry axis and the bending of cross-section about the perpendicular axis (x-axis) is treated as the curvature (c_x) of the long profile. The standard elasto-plastic stress-strain operator is given as

$$\hat{\mathbf{C}}^{\text{ep}}_{\text{std}} = 3\kappa\hat{\mathbf{P}}_1 + 2\mu\hat{\mathbf{P}}_2 - \frac{2\mu}{1+\frac{H}{3\mu}}\hat{\mathbf{n}}'_{\mathbf{T}} \tag{39}$$

where $\hat{\mathbf{P}}_1$ is the spherical projector, $\hat{\mathbf{P}}_2$ is the deviator projector, and $\hat{\mathbf{n}}'_{\mathbf{T}}$ is the plastic flow direction projector. The projectors for the beam cross-sectional elements are of size 4 × 4

$$\hat{\mathbf{P}}_1 = \frac{1}{3}\begin{bmatrix} 1 & 1 & 0 & 1 \\ 1 & 1 & 0 & 1 \\ 0 & 0 & 0 & 0 \\ 1 & 1 & 0 & 1 \end{bmatrix}, \quad \hat{\mathbf{P}}_2 = \frac{1}{2}\begin{bmatrix} +\frac{4}{3} & -\frac{2}{3} & 0 & -\frac{2}{3} \\ -\frac{2}{3} & +\frac{4}{3} & 0 & -\frac{2}{3} \\ 0 & 0 & 1 & 0 \\ -\frac{2}{3} & -\frac{2}{3} & 0 & +\frac{4}{3} \end{bmatrix}. \tag{40}$$

4. Results and discussions

The proposed thermo-mechano-metallurgical model is validated for the beam quenching experiment conducted by Newman et al. (2003). The evolution of curvature is simulated using the present model, and compared with the experimental result of Newman et al. (2003), and numerical results of Newman et al. (2003) as shown in Fig. 3. A rectangular cross-sectional (20 mm × 60 mm) beam made up of W319 aluminum with simply supported boundary conditions at the ends, having a length of 306 mm is partially immersed in a water bath and its displacement is measured through LVDT. Through the measurement of temperature profiles at selected locations, an inverse problem (Nallathambi and Specht, 2009) has to be solved for the estimation of heat transfer coefficients. The boundary conditions and some of the material properties of W319 aluminum can be found in the reference Newman et al. (2003). Result shows that the present model qualitatively agree with the experimental result. Due to the lack of appropriate material properties, the present model result lacks to fit quantitatively with the experimental, and numerical results of Newman et al. (2003). Further, Newman et al. (2003) used the stress based mechanical threshold stress Voce formulation which is different from the present model. However, this verification is

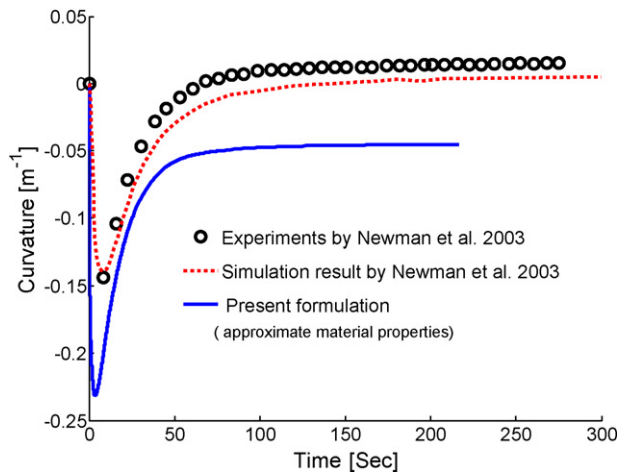

Fig. 3. Curvature evolution: beam quenching experiment by Newman et al. (2003).

good enough and strengthened to study the influence of material properties on the final distortion and residual stresses.

An L120 × 12 profile made up of 100Cr6 steel at 900° C which fully consists of austenite is considered for the understanding of the percentage change in each properties on curvature and stresses. The temperature-dependent material properties of the individual phases can be found in reference Pietzsch et al. (2007). Equal cooling with HTC of 1000 W/m^2 K is treated as the thermal boundary condition of the L cross-section having unit length and the FE mesh is shown in Fig. 4.

A simply supported boundary condition with zero initial curvature (c_x) is assigned as the mechanical boundary condition. Axis-symmetric boundary condition with zero moment ($M_y = 0$) is assigned on the nodes lying in the symmetry axis (y-axis). Further, the x and y displacements of node lying at the origin (auxiliary node) is arrested.

The material properties are grouped according to the physical fields: thermal, metallurgical, and mechanical material properties. The final curvature (c_x) of the structure is treated as a measure of distortion, and a volume averaged mean effective stress ($\sigma^{\text{avg}}_{\text{eff}}$) is considered for the residual stresses. The material property under investigation is multiplied by a factor which varies from 0.8 to 1.2 (with an increment of 0.1), and the respective final distortion and

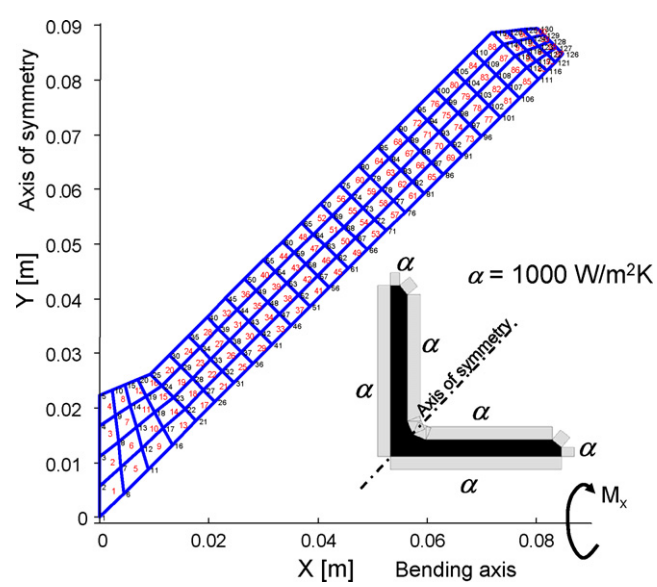

Fig. 4. An L120 × 12 profile considered for analysis and its FE mesh.

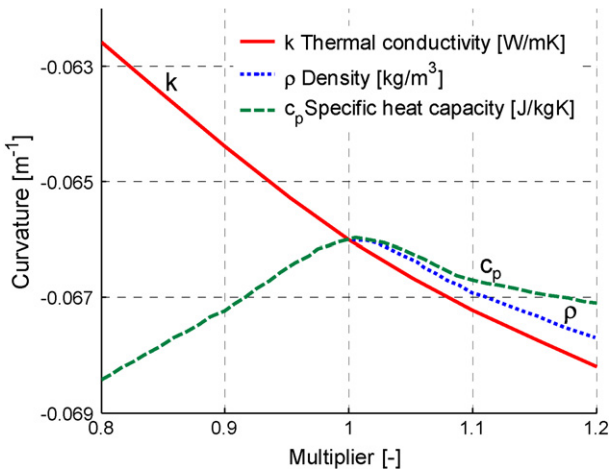

Fig. 5. Sensitivity of thermal properties on curvature.

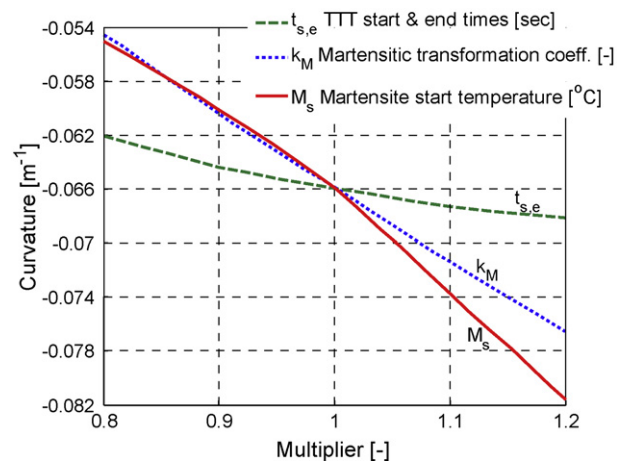

Fig. 7. Sensitivity of metallurgical properties on curvature.

residual stresses are calculated by sequentially solving the above mentioned physical fields using an isothermal staggered approach.

4.1. Thermal properties

The thermal conductivity (k), the density (ρ), and the specific heat capacity (c_p) are the thermal material properties which play a key role in the energy equation (Eq. (1)). The sensitivity of the distortion and residual stresses are plotted as shown in Figs. 5 and 6, respectively. It shows that the thermal conductivity of the quenched metal is dominating over the other thermal properties on the curvature and stress. An almost direct linear change in curvature is obtained for the variation of the thermal conductivity from $0.8k$ to $1.2k$. In contrast to k, ρ and c_p form a non-linear relation as shown in Fig. 5. But all the thermal properties produce negative slopes in the $\sigma_{\text{eff}}^{\text{avg}}$ vs. multiplier plot as shown in Fig. 6. In overall, increase in all the thermal parameter decreases the effective stress, but the curvature increases, which is not favorable for the efficient heat treatment process.

4.2. Metallurgical properties

The TRIP strain (Leblond, 1989; Kobayashi and Yamamoto, 1988) has a great influence on the distortion and residual stresses. Therefore, TRIP effects should be included in the model to obtain realistic and reliable simulation results. The Greenwood–Johnson coefficient (Λ_j) is the only metallurgical material property which controls the TRIP strain. It can be approximated by using the density and the yield stress (Leblond, 1989). The other important metallurgical properties having influence on the distortion and the residual stresses are t_s and t_e in the TTT diagram, the martensitic transformation coefficient (k_M) and the martensite transformation start time (M_s) as shown in Figs. 7 and 8, respectively. All metallurgical properties having an almost linear relationship with c_x and $\sigma_{\text{eff}}^{\text{avg}}$ as shown in Figs. 7 and 8. M_s has a higher influence apart from the others. The decrease in M_s significantly reduces the c_x and $\sigma_{\text{eff}}^{\text{avg}}$, which can be achieved by an increase of the carbon content. The physics behind the decrease in M_s and the martensite transformation interval are discussed in detail by Todinov (1999). Followed by M_s, k_M has a medium influence, and the t_s and t_e are showing the least influence on c_x and $\sigma_{\text{eff}}^{\text{avg}}$. The interesting point to be noted here is that a reduction in all the metallurgical properties simultaneously reduce the curvature and effective stress, which is an important information for the metallurgists.

4.3. Mechanical properties

The bulk modulus (κ), the shear modulus (μ), the initial yield stress (σ_y), and the hardening modulus (H) are the four important mechanical parameters influencing the quenching distortion and residual stresses as shown in Figs. 9 and 10, respectively.

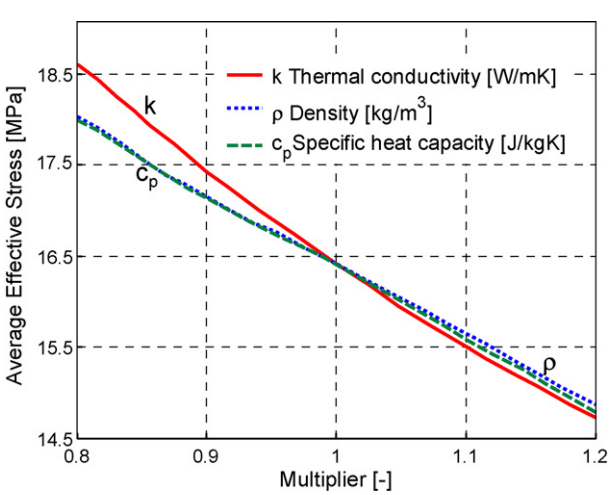

Fig. 6. Sensitivity of thermal properties on average effective stress.

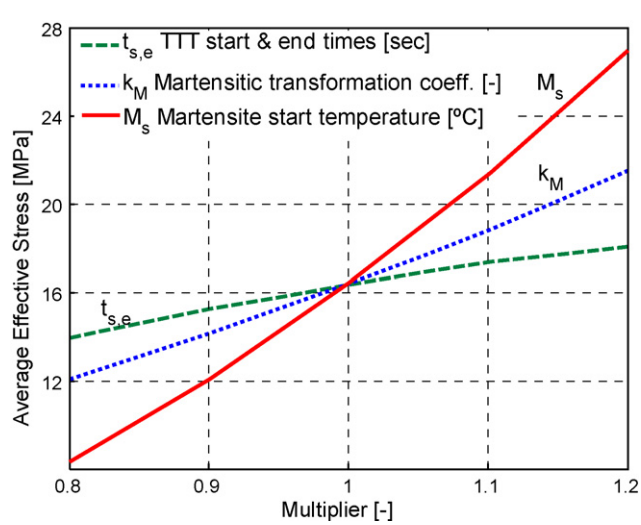

Fig. 8. Sensitivity of metallurgical properties on average effective stress.

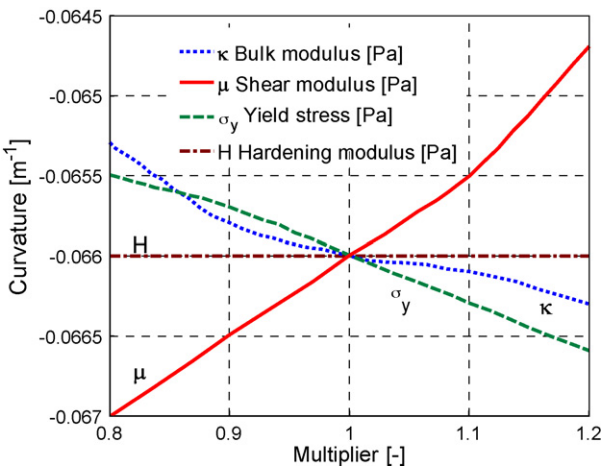

Fig. 9. Sensitivity of mechanical properties on curvature.

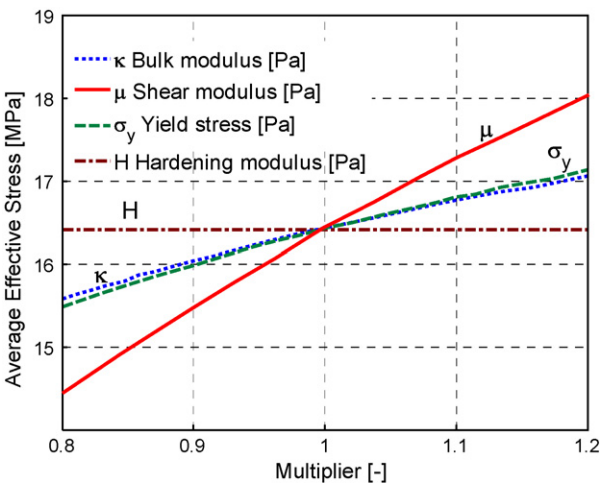

Fig. 10. Sensitivity of mechanical properties on average effective stress.

κ and μ are used to describe the stress–strain relation in the elastic range and additionally μ and H are used once the material starts yielding. It is perceived that the influence of H on the distortion and the residual stresses are almost null as shown in Figs. 9 and 10. μ is the material property with the strongest effect upon quenching. A slightly non-linear relationship between μ and c_x is perceived. Increase in μ decreases c_x which is not the case for σ_y and κ. σ_y and κ behave identically with respect to $\sigma_{\text{eff}}^{\text{avg}}$ as shown in Fig. 10. κ is related to the volumetric change under stress so it does not influence the plastic deformations. A decrease in the bulk modulus and the yield stress simultaneously lower the curvature and the effective stress which is highly preferred.

5. Concluding remarks

The sensitivity analyses of the material properties on the curvature and residual stresses during the quenching processes are performed. A rate-independent, small deformation thermo-elasto-plastic material model with temperature and phase fraction-dependent material properties is implemented in the study. The newly developed beam cross-sectional element delivers the curvature of long profiles. The thermal conductivity, martensitic start temperature, and shear modulus are the dominant material properties which have strong influence on curvature and effective stresses. It is demonstrated that the hardening modulus has no influence on both the distortion and residual stresses. This sensitivity analysis shows that the change in none of the thermal properties simultaneously reduce the distortion and residual stresses. Simultaneous reduction in curvature and average effective stress is possible through the reduced metallurgical properties, yield stress, and bulk modulus.

Acknowledgment

The financial support provided by the German Science Foundation (DFG) through GKMM 828 graduate school is sincerely acknowledged.

References

Andrade-Campos, A., Neto da Silva, F., Teixeira-Dias, F., 2007. Modelling and numerical analysis of heart treatments on aluminium parts. International Journal for Numerical Methods in Engineering 70 (5), 582–609.
Argyris, J.H., Doltsinis, J.S., 1981. On the natural formulation and analysis of large deformation coupled thermomechanical problems. Computer Methods in Applied Mechanics and Engineering 25 (2), 195–253.
Armero, F., Simo, J.C., 1992. A new unconditionally stable fractional step method for nonlinear coupled thermomechanical problems. International Journal for Numerical Methods in Engineering 35 (4), 737–766.
Avrami, M., 1939. Kinetics of phase change i. Journal of Chemical Physics 7, 1103–1112.
Barka, N., Bocher, P., Brousseau, J., Galopin, M., Sundararajan, S., 2007. Modeling and sensitivity study of the induction hardening process. Advanced Materials Research, 15–17, 525–530.
Bathe, K.J., 1996. Finite Element Procedures, fifth edition. Prentice-Hall Inc., New Jersey.
Batista, M., Kosel, F., 2000. A sensitivity analysis of the heat treatment of steel. Strojniski Vestnik/Journal of Mechanical Engineering 46 (11–12), 718–731.
Bertram, A., Böhlke, T., Šilhavý, M., 2007. On the rank 1 convexity of stored energy functions of physically linear stress–strain relations. Journal of Elasticity 86 (3), 235–243.
Brzoza, M., Specht, E., Ohland, J., Belkessam, O., Lübben, T., Fritsching, U., 2006. Minimizing stress and distortion for shafts and discs by controlled quenching in a field of nozzels. Materials Science and Engineering Technology 37, 97–102.
Chen, W.F., 1994. Constitutive Equations for Engineering Materials, vol. 2, Plasticity and Modelling. Elsevier, The Netherlands.
Chuzhoy, L., Cai, J., Sharma, R.K., Rivera, E.J., Li, M., Burris, K.W., Johnson, M.L., Henyei Jr., G., 2003. Application of numerical methods to quantitative characterization of production quenches. 58th Congresso Anual da ABM (ASSociacao Brasileira de Metalurgia e Materiais), 3477–3483.
Ferguson, B.L., Freborg, A.M., Petrus, G.J., 2001. Modeling to investigate sensitivities to heat treat process variables. ASM Proceedings: Heat Treating, 214–219.
Freborg, A.M., Li, Z., Ferguson, B.L., 2007. Assessing heat treatment distortion sensitivity. ASM International – 24th Heat Treating Society Conference 2007, Driving the Engines of Change in Manufacturing, 115–125.
Friesenbichler, C., Wieser, V., Redi, C., 2006. Heat treatment of hot work tool steel—a sensitivity analysis. Proceedings – 15th IFHTSE – International Federation for Heat Treatment and Surface Engineering Congress, 379–383.
Greenwood, G.W., Johnson, R.H., 1965. The deformation of metals under small stress during phase transformation. Proceedings of the Royal Science A283, 403–422.
Johnson, W.A., Mehl, R.F., 1939. Reaction kinetics in processes of nucleation and growth. Transactions of AIME 135, 416–458.
Kang, S.H., Im, Y.T., 2007. Finite element investigation of multi-phase transformation within carburized carbon steel. Journal of Materials Processing Technology 183, 241–248.
Kaymak, Y., 2007. Modeling of metal quenching process and strategies to minimize distortion and stresses, Ph.D. Thesis, Otto von Guericke University Magdeburg, Germany.
Kaymak, Y., Specht, E., 2007. Strategies for controlled quenching to reduce stresses and distortion. Heat Processing 5 (3), 1–4.
Kobayashi, T., Yamamoto, H., 1988. Development of high toughness in austempered type ductile cast iron and evaluation of its properties. Metallurgical Transactions A 19 (2), 319–327.
Koistinen, D.P., Marburger, R.E., 1959. A general equation prescribing the extent of the austenite–martensite transformation in pure iron–carbon alloys and plain carbon steels. Acta Metallica 7 (1), 59–60.
Leblond, J.B., 1989. Mathematical modelling of transformation plasticity in steels. ii: Coupling with strain hardening phenomena. International Journal of Plasticity 5 (6), 573–591.
Li, Z., Freborg, A.M., Ferguson, B.L., 2007. Effective design of heat treat processes using computer simulations, ASM International – 24th Heat Treating Society Conference 2007, Driving the Engines of Change in Manufacturing, 205–213.
Mirzaee-Sisan, A., Smith, D.J., Truman, C.E., 2007. Characterizing residual stresses in rectangular beam specimens following thermomechanical loading. Journal of Strain Analysis for Engineering Design 42 (2), 79–93.
Nallathambi, A.K., Kaymak, Y., Specht, E., Bertram, A., 2008. Distortion and Residual Stresses during Metal Quenching Process. In: Bertram, A., Thomas, J. (Eds.),

Micro-Macro-Interactions in Structured Media and Particle Systems. Springer, Berlin Heidelberg, pp. 145–157, doi:10.1007/978-3-540-85715-0-12.
Nallathambi, A.K., Kaymak, Y., Specht, E., Bertram, A., 2009. Optimum strategies to reduce residual stresses and distortion during metal quenching process. Journal of ASTM International 6 (4).
Nallathambi, A.K., Specht, E., 2009. Estimation of heat flux in array of jets quenching using experimental and inverse finite element method. Journal of Materials Processing Technology 209 (12–13), 5325–5332.
Newman, M.L., Robinson, B.J., Sehitoglu, H., Dantzig, J.A., 2003. Deformation, residual stress, and constitutive relations for quenched w319 aluminum. Metallurgical and Materials Transactions A 34A, 1483–1491.
Pietzsch, R., Brzoza, M., Kaymak, Y., Specht, E., Bertram, A., 2005. Minimizing the distortion of steel profiles by controlled cooling. Steel Research International 76, 399–407.
Pietzsch, R., Brzoza, M., Kaymak, Y., Specht, E., Bertram, A., 2007. Simulation of the distortion of long steel profiles during cooling. Journal of Applied Mechanics 74, 427–437.
Scheil, E., 1935. Anlaufzeit der austenitumwandlung. Archiv fur das Eisenhuttenwesen 12, 564–567.
Simo, J.C., Hughes, T.J.R., 1997. Computational Inelasticity. Springer Verlag, New York.
Sjostrom, S., 1984. Interactions and constitutive models for calculating quench stresses in steel. Materials Science and Technology 1 (10), 823–829.
Smoljan, B., 2002. Numerical simulation of steel quenching. Journal of Materials Engineering and Performance 11 (1), 75–79.
Song, J., Peters, J., Noor, A., Michaleris, P., 2003. Sensitivity analysis of the thermomechanical response of welded joints. International Journal of Solids and Structures 40 (16), 4167–4180.
Todinov, M.T., 1999. Influence of some parameters on the residual stresses from quenching. Modelling and Simulation in Materials Science and Engineering 7, 25–41.
Totten, G.E., Bates, C.E., Clinton, N.A., 1993. Handbook of Quenchants and Quenching Technology. ASM International, Metals Park.